Evaluation of Gamma Raindrop Size Distribution Assumption through Comparison of Rain Rates of Measured and Radar-Equivalent Gamma DSD

ELISA ADIROSI

Institute of Atmospheric Sciences and Climate, Italian National Research Council (CNR), and Department of Civil, Building and Environmental Engineering, Sapienza University of Rome, Rome, Italy

EUGENIO GORGUCCI AND LUCA BALDINI

Institute of Atmospheric Sciences and Climate, Italian National Research Council (CNR), Rome, Italy

ALI TOKAY

Joint Center for Earth Systems Technology, University of Maryland Baltimore County, Catonsville, and NASA Goddard Space Flight Center, Greenbelt, Maryland

(Manuscript received 24 April 2013, in final form 3 February 2014)

ABSTRACT

To date, one of the most widely used parametric forms for modeling raindrop size distribution (DSD) is the three-parameter gamma. The aim of this paper is to analyze the error of assuming such parametric form to model the natural DSDs. To achieve this goal, a methodology is set up to compare the rain rate obtained from a disdrometer-measured drop size distribution with the rain rate of a gamma drop size distribution that produces the same triplets of dual-polarization radar measurements, namely reflectivity factor, differential reflectivity, and specific differential phase shift. In such a way, any differences between the values of the two rain rates will provide information about how well the gamma distribution fits the measured precipitation. The difference between rain rates is analyzed in terms of normalized standard error and normalized bias using different radar frequencies, drop shape–size relations, and disdrometer integration time. The study is performed using four datasets of DSDs collected by two-dimensional video disdrometers deployed in Huntsville (Alabama) and in three different prelaunch campaigns of the NASA–Japan Aerospace Exploration Agency (JAXA) Global Precipitation Measurement (GPM) ground validation program including the Hydrological Cycle in Mediterranean Experiment (HyMeX) special observation period (SOP) 1 field campaign in Rome. The results show that differences in rain rates of the disdrometer DSD and the gamma DSD determining the same dual-polarization radar measurements exist and exceed those related to the methodology itself and to the disdrometer sampling error, supporting the finding that there is an error associated with the gamma DSD assumption.

1. Introduction

Accurate characterization and modeling of raindrop size distribution (DSD) are required to understand rain microphysics and develop rain retrieval algorithms. In radar meteorology, precipitation retrieval algorithms often rely on regression methods on precipitation parameters and corresponding simulated radar measurements computed assuming widely varying distributions of gamma DSDs (e.g., Bringi and Chandrasekar 2001, section 8.1.1). This approach assumes that radar always samples raindrops whose sizes follow a gamma distribution from which both precipitation observables, such as rain rate or liquid water content, and, with further assumptions, radar measurements can be computed. Weather radar applications, such as quantitative precipitation estimation or precipitation microphysics retrieval, are not the only applications affected by this assumption. In general, in addition to remote sensing precipitation retrieval, the choice of DSD shape plays a central role in data assimilation since it affects the error matrix of instruments to be assimilated. A DSD is the result of

Corresponding author address: Luca Baldini, Consiglio Nazionale delle Ricerche, Istituto di Scienze dell'Atmosfera e del Clima, Area della Ricerca Roma 2 Tor Vergata, Via Fosso del Cavaliere, 100, I-00133 Rome, Italy.
E-mail: l.baldini@isac.cnr.it

DOI: 10.1175/JAMC-D-13-0150.1

© 2014 American Meteorological Society

different physical processes such as coalescence, aggregation, and breakup involved in the formation and evolution of rain. Because of variability of these processes, a single, explicit, parametrical functional form may not represent adequately all the natural DSDs. Indeed, different functions have been used to model DSD. Historically, a specific form of exponential DSD (Marshall and Palmer 1948) has been the first analytical parameterization used. Ulbrich (1983) found that the exponential model is a very good approximation of the DSD when a sufficient averaging in space and/or time is performed, whereas in the other cases the exponential DSD overestimates the number of both very small and very large drops (Gunn and Marshall 1955; Joss and Gori 1978). To overcome this problem and to describe a wider range of drop size distributions, Ulbrich (1983) suggested modeling the DSD using the three-parameter gamma distribution

$$N(D) = N_0 D^{\mu} \exp(-\Lambda D), \tag{1}$$

where $N(D)$ is the expected number of drops per unit of drop diameter interval and per unit volume; D (mm) is the diameter of a sphere with the same volume as a raindrop; and μ (mm^{-1}), Λ (mm^{-1}), and N_0 ($\mathrm{mm}^{-1-\mu}\,\mathrm{m}^{-3}$), are the shape, the slope, and the intercept parameters, respectively.

Although there are in literature several different parametric forms to model the measured DSD, such as Weibull distribution (Best 1950), lognormal distribution (Feingold and Levin 1986), or scaling law (Sempere Torres at al. 1994), to date the three-parameter gamma distribution is widely accepted and used by radar meteorologists and atmospheric physicists to model natural DSDs (Chandrasekar and Bringi 1987; Kozu and Nakamura 1991; Tokay et al. 2001; Zhang et al. 2003; Smith et al. 2009). However, it is feasible that actual DSDs cannot be well represented by the gamma function (Adirosi et al. 2013; Ignaccolo and De Michele 2014). A common technique for deriving the three parameters from a measured drop spectra is the method of moments, which consists in identifying the parameters of the gamma DSD that have the same three statistical moments of a given disdrometer-measured spectrum. Different methods depending on the different choice of moments have been proposed [e.g., Tokay and Short (1996) used the third, fourth, and sixth moments, while Caracciolo et al. (2006) used the fourth, fifth, and sixth moments]. If, for instance, the third moment is used, the obtained gamma distribution will have the same liquid water content as the measured DSD. However, Smith and Kliche (2005) found that the method of moments provides biased results, and that the error increases as the order of moments used increases, whereas Kliche et al. (2008), comparing the moment method estimators with the L-moment (Hosking 1990) and the maximum likelihood estimators, found that the last two methods give better results when untruncated DSDs are considered. Cao and Zhang (2009) used simulated and measured DSDs to investigate the performances of seven different estimation methods of gamma DSD parameters and concluded that, because of the lack of measurements of small drops, it is better to avoid the use of the L-moment and maximum likelihood method to process the disdrometer-measured data.

Therefore, efforts have been made to find the optimal estimator of DSD parameters based on the assumption that the natural DSDs follow the gamma distribution. Cao and Zhang (2009), evaluating the performances of different estimators, investigated the effect of disdrometer measurement error and gamma model assumption on integral parameters such as the rain rate. Instead, the proposed approach evaluates the validity of the gamma DSD assumption through comparison between the disdrometer-measured DSD and the simulated gamma DSD that provides the same set of dual-polarization radar measurements. The three parameters of the gamma DSD are found to represent a measured drop spectrum if they produce the same triplet of dual-polarization radar measurements, namely, reflectivity factor at horizontal polarization (Z_h), differential reflectivity (Z_{dr}), and the specific differential phase shift (K_{dp}). The rain rates of two DSDs are then compared. Part of the difference in terms of rain rate is ascribed to the gamma DSD functional form assumption, and it can been seen as a proxy of the error related to the assumption that the natural DSDs are gamma shaped. It should be noted that this approach is generic and can be easily applied to any other analytical functional forms used to model the natural DSDs. Moreover, the influence of different assumptions—such as the raindrop shape model, the integration time interval, the radar frequency, and the influence of disdrometer sampling error—has been investigated.

The disdrometer measurements used in this analysis were collected by 2D video disdrometers in a variety of climate regimes. Four different datasets are considered: one collected at Huntsville, Alabama; and three collected during the prelaunch Global Precipitation Measurement (GPM) Mission field campaigns in Finland, Oklahoma, and central Italy.

The paper is organized as follows: Section 2 provides a summary of the background theory related to problem addressed in this paper; the methodology to retrieve the gamma DSD parameter is introduced in section 3. In section 4 there is a description of the measured (section 4a) and simulated (section 4b) datasets used to validate the methodology, and the results are presented in section 5.

The important results and conclusions are found in section 6.

2. Theoretical background

The gamma drop size distribution ($\mathrm{mm^{-1}\,m^{-3}}$) can be written in terms of the probability density of the raindrops as

$$N(D) = n_c \frac{\Lambda^{\mu+1}}{\Gamma(\mu+1)} e^{-\Lambda D} D^{\mu}, \tag{2}$$

where n_c ($\mathrm{mm^{-3}}$) is the concentration of raindrops, and Γ indicates the gamma function. From this fundamental notion of the drop size distribution, any other gamma form can be derived, such as Eq. (1). Willis (1984) gave an alternative formulation of the DSD that is useful for comparing DSDs that have different values of liquid water content, known as normalized gamma DSD, and expressed as

$$N(D) = N_w f(\mu) \left(\frac{D}{D_0}\right)^{\mu} \exp\left[-(3.67+\mu)\left(\frac{D}{D_0}\right)\right], \tag{3a}$$

$$f(\mu) = \frac{6}{(3.67)^4} \frac{(3.67+\mu)^{\mu+4}}{\Gamma(\mu+4)}, \tag{3b}$$

where N_w ($\mathrm{mm^{-1}\,m^{-3}}$) is the "intercept" parameter of a normalized gamma drop size distribution and D_0 (mm) is the mass-weighted median diameter. These derivations [Eqs. (2) and (3a)] are based on complete gamma function where the integral extends from 0 to infinity. In reality, the observed DSDs are bounded by the minimum ($D_{\min}$) and the maximum ($D_{\max}$) drop diameters (Ulbrich 1985). The three parameters of the normalized gamma (N_w, D_0, and μ) define a gamma $N(D)$ from which it is possible to compute both rain parameters such as the rainfall rate or the liquid water content, and, introducing further assumptions and using an electromagnetic model, radar measurements such as the horizontal reflectivity, the differential reflectivity, and the specific differential propagation phase. The rain rate can be expressed as

$$R = 6\pi 10^{-4} \int_0^{\infty} v(D) N(D) D^3\, dD \quad (\mathrm{mm\,h^{-1}}), \tag{4}$$

where $v(D)$ is the terminal fall speed of a drop as a function of drop diameter. A widely used $v(D)$ relation is given by Gunn and Kinzer (1949) as

$$v(D) = 9.65 - 10.3 \exp(-0.6D) \quad (\mathrm{m\,s^{-1}}). \tag{5}$$

Concerning radar measurements, the reflectivity factor at horizontal and vertical polarization can be expressed through $N(D)$ as

$$Z_{h,v} = \frac{4\lambda^4}{\pi^4 |K_w|^2} \int |s_{h,v}(D)|^2 N(D)\, dD \quad (\mathrm{mm^6\,m^{-3}}), \tag{6}$$

where λ is the wavelength, $K_w = (\varepsilon_r - 1)(\varepsilon_r + 2)^{-1}$, ε_r is the complex dielectric constant of water, and $s_{h,v}(D)$ are the backscattering amplitudes at horizontal and vertical polarizations (denoted by the subscripts h and v, respectively) that depend on size, shape, and orientation of the raindrop. The other radar measurements used in this study are the differential reflectivity defined as the ratio of the reflectivity factor at the horizontal and vertical polarizations and expressed by

$$Z_{\mathrm{dr}} = 10 \log_{10} \frac{\int |s_h(D)|^2 N(D)\, dD}{\int |s_v(D)|^2 N(D)\, dD} \quad (\mathrm{dB}), \tag{7}$$

and the specific differential propagation phase shift that can be computed as

$$K_{\mathrm{dp}} = \frac{180\lambda}{\pi} \int \mathrm{Re}[f_h(D) - f_v(D)] N(D)\, dD \quad (^{\circ}\,\mathrm{km^{-1}}), \tag{8}$$

where $f_{h,v}(D)$ are the forward-scattering amplitudes.

When the Rayleigh assumption ($D \ll \lambda$; i.e., diameter of the drop is much smaller than the wavelength of the incident electromagnetic radiation) is not valid, back- and forward-scattering cross-section areas can be obtained using electromagnetic simulation such as the T-matrix method, based on the algorithm developed by Barber and Yen (1975). Among the assumptions required to perform this simulation, one concerns the relation used to describe the drop axis ratio as a function of drop equivalent diameters. In practice, the shape of drops is approximated by an oblate spheroid with the same volume of the drop and axis ratio b/a, where b and a are the vertical and the horizontal axes of the raindrop, respectively. Several different shape models have been presented and discussed in the literature (see Beard et al. 2010, for an overview). In this paper the following models are used: 1) the relation of Pruppacher and Beard (1970) that was obtained from a linear fit to wind tunnel data (labeled as PB in this paper), 2) the equilibrium relation of Beard and Chuang (1987) (labeled as BC), 3) the experimental relation in Brandes et al. (2002) (labeled as Br), and 4) the linear relations $b/a = (1.03 - \beta D)$ proposed by Gorgucci et al. (2000) with the values of $\beta = 0.05$ and 0.07 (herein labeled SL05 and SL07, respectively).

3. Methodology

The proposed method determines, for a measured DSD, the corresponding gamma DSD that gives the same radar measurement triplet (Z_h, Z_{dr}, and K_{dp}). In this study we avoid to use a DSD parameter estimation method, but the gamma DSDs are computed by the simulation procedure described in section 4b. Given a disdrometer-measured DSD, the corresponding radar reflectivity ($Z_{h,m}$), differential reflectivity ($Z_{dr,m}$), and specific differential propagation phase ($K_{dp,m}$) are computed using the T-matrix method (the subscript m indicates that measurements were obtained from measured DSDs) and will be called as the "measured" triplet. The rain rate of the measured DSD (R_m) is also computed with Eq. (4). An appropriately wide set of the three gamma DSD parameters was generated as shown below, and using the same assumptions, the corresponding triplet of radar observables ($Z_{h,s}$, $Z_{dr,s}$, and $K_{dp,s}$) were obtained from the T-matrix method. This gamma DSD dataset will be referred to as the simulated dataset and its radar triplets and corresponding rain rates (R_s), computed using Eq. (4), are identified by the subscript s and discussed in detail in section 4b.

The criterion to match radar triplets computed from measured spectra with triplets computed from gamma DSDs is obtained by combining two different procedures: the first one uses a cost function to identify the nearest-neighbor radar measurement triplet in the simulated dataset, while the second one uses a 3D interpolating function. The cost function is

$$\mathrm{CF} = \frac{(Z_{h,m} - Z_{h,s})^2}{\overline{Z_{h,s}}} + \frac{(Z_{dr,m} - Z_{dr,s})^2}{\overline{Z_{dr,s}}} + \frac{(K_{dp,m} - K_{dp,s})^2}{\overline{K_{dp,s}}} \tag{9}$$

and describes the distance between two points in the 3D space defined by the three radar measurements Z_h, Z_{dr}, and K_{dp}, normalized by the mean of their values in the simulated dataset ($\overline{Z_{h,s}}$, $\overline{Z_{dr,s}}$, and $\overline{K_{dr,s}}$, respectively). Selecting the triplet in the set of the simulated database that minimizes Eq. (9) permits finding the gamma DSD that matches the given measured DSD. To obtain a meaningful match, the minimum distance between a measured and a simulated triplet has been defined to be equal to or lower than 0.001. In other words, a triplet of radar observables from measured DSD can be considered as matched to a triplet of radar observables of the simulated dataset only if the distance between the two observables in the space defined above is less than 0.001. Otherwise, the measured triplet is discarded. This means that the given measured triplet, and consequently the given measured DSD, is considered as not represented in the gamma-simulated dataset. When the values of rain rates of the gamma DSDs located, in the 3D space defined by the three radar measurements, around the measured DSD are not homogeneous (difference between maximum and minimum value greater than 15 mm h^{-1}) the matching is considered unreliable, since a small change in the value of the radar triplet can cause a relatively large change in the value of the rain rate. In this subvolume of the 3D space of the radar measurement triplets, either the proposed methodology is not robust enough or the simulated dataset is not dense or is not wide enough to represent adequately that DSD.

For interpolation purposes, an unstructured mesh in the 3D space is generated by the Delaunay (1934) triangulation method. A function that fits a surface of the form $R_s = f(Z_{h,s}, Z_{dr,s}, K_{dp,s})$ to the scatter data $Z_{h,s}$, $Z_{dr,s}$, $K_{dp,s}$, and R_s is obtained. The latter interpolating function does not extrapolate outside the convex hull of the data with which it has been built.

Knowing the two values of the simulated rain rates obtained using both the cost function and the interpolating function, a quality control is applied. The measured triplet is discarded if the difference in terms of rain rate between the results of the two methods is greater than 4 mm h^{-1}. In this condition, the method is not able to detect a gamma DSD that can be compared with the measured DSD. This control is added because, near the border of the 3D space of the radar measurements, triplets are quite sparse; thus, both the nearest neighbor selected via cost function and the interpolating function can give an erroneous result. Verifying the agreement between the two methods overcomes this problem. It will be shown later that the number of the measured DSDs that are discarded from the considered measured dataset changes depending on the shape model and the integration time, and its value is low. The percentages range between 2% and 7% for C band, while for S band and X band the percentages are slightly lower. It is important to point out that in selecting measured DSDs, the criterion based on the cost function threshold (CF $<$ 0.001) plays the most important role. In fact, the percentage of discarded DSDs due to quality control is around 1% or less for all the datasets; such a percentage corresponds to a number of discarded DSDs equal to one or two, and at maximum fewer than five.

Cao and Zhang (2009) evaluated the performances of different estimation methods (i.e., method of moments with different sets of moments, L-moment and maximum likelihood) to analyze the effect of measurement and model error. The method of moments is based on equations that can be solved in closed forms, whereas for

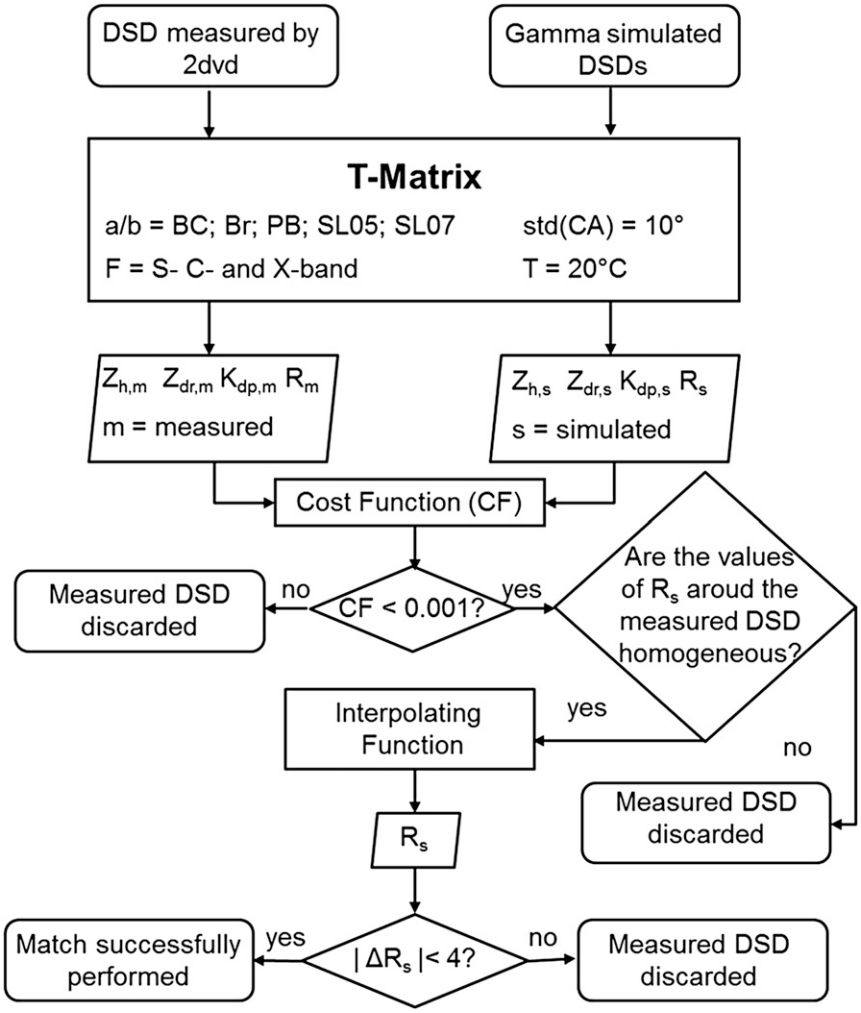

FIG. 1. Flowchart summarizing the methodology for deriving a gamma DSD equivalent to measured DSD spectra in terms of dual-polarization radar measurements (Z_h, Z_{dr}, and K_{dp}).

the method described above it is necessary to devise an approximated procedure to map the 3D space of radar measurements onto the space of the three parameters of gamma DSD based on the cost function Eq. (9) and the Delaunay triangulations in a set of known gamma DSDs to determine the corresponding rain rate. In this way we can find a pair of DSDs (i.e., one measured and one simulated gamma) that under similar assumptions determine the same triplet of polarimetric radar measurements. The flowchart in Fig. 1 provides an overview of the method used along with the main assumptions adopted.

4. Data

This study uses DSDs measured by several two-dimensional video disdrometers along with a set of gamma DSDs with widely variable parameters. In this section a brief description of the instrument used for the measurements is discussed. Moreover, both the analysis techniques performed on the measured dataset to remove the spurious drops and on the simulated dataset to define the ranges of variability of the gamma DSD parameters are discussed.

a. Disdrometer-measured DSD datasets

The measured raindrop spectra were collected with a 2D video disdrometer, an optical device manufactured by Joanneum Research in Graz, Austria (Schönhuber et al. 2008). It uses two orthogonal light sheets that are projected onto two line-scan cameras. A drop that falls through the light sheet casts shadows on the photodetectors. The matching of the same drops falling into the planes is critical to identify the correct size, fall velocity,

and shape of the individual hydrometeors. The manufacturer software outputs the time stamp of an individual hydrometeor with its equivalent diameter, fall velocity, and oblateness. The height and the width of the particle and position in each plane are also given. The virtual measuring area is nominally $10 \times 10\,\mathrm{cm}^2$.

In general, the principal limitations in disdrometer measurements are sampling error related to small sampling volumes, splashing (Tokay et al. 2001), and wind effects (Nešpor et al. 2000). Physical variations and statistical sampling errors coexist and it is difficult to separate them with a single instrument (Cao et al. 2008; Tokay et al. 2013). The two-dimensional video disdrometer (2DVD) provides potentially an accurate description of drop size spectra and has been employed in several field campaigns around the world (Tokay et al. 2001; Bringi et al. 2003; Zhang et al. 2011). It has to be underlined that the third generation (compact version) of 2DVD was used in this study. This version is designed to improve the alignment of the optical components and the grid resolution and to mitigate splashing and wind effects (Schönhuber et al. 2007).

Typically, there are a number of outliers measured by the 2DVD that result in particles having velocity or oblateness that are highly different from expected values. These outliers (or spurious drops) may be due to splashing or wind effect and their number increases in heavy rain conditions. Another potential cause of an outlier is the increases of nonaxisymmetric oscillations (Thurai et al. 2013); these oscillations can cause the 2DVD drop matching to fail. In this study the mismatched drops are removed by considering the drops outside ±50% of the Gunn and Kinzer (1949) size–fall velocity relation to be eliminated (Tokay et al. 2001). As an example, Fig. 2a shows the relation between diameter and fall velocity for 2DVD data collected by one of the disdrometers used in this study [it is one of the disdrometers deployed in Oklahoma during the Midlatitude Continental Convective Clouds Experiment (MC3E) field campaign], with the gray line describing the relation of Gunn and Kinzer (1949). The dataset, before the application of the velocity filter, is composed of more than 800 000 drops. While Fig. 2b shows the effect of the filtering that reduces the drops to about 690 000. The percentages of spurious drops eliminated by this filtering are 15.5%, 8.9%, 11.3%, and 14.2% for the National Space Science and Technology Center (NSSTC), Light Precipitation Validation Experiment (LPVEx), MC3E, and Hydrological Cycle in Mediterranean Experiment (HyMeX) datasets, respectively. The simultaneous presence of 10 drops and rain rate $> 0.01\,\mathrm{mm\,h^{-1}}$ were the criteria for rain/no rain discrimination.

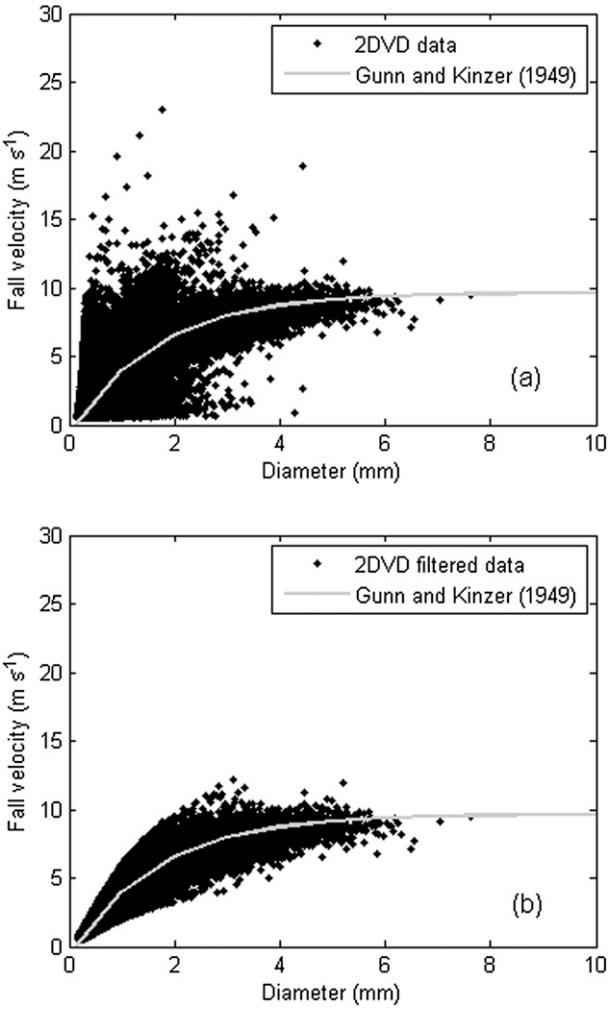

FIG. 2. Relation between drop diameter and fall velocity in 2DVD data (a) before and (b) after the application of the filter criteria proposed by Tokay et al. (2001). The gray line is the theoretical drop shape–size relation of Gunn and Kinzer (1949). The 2DVD data are from one of the disdrometers deployed in Oklahoma during the MC3E field campaign.

As previously mentioned, considered are data collected by 2DVDs located at four different sites, namely (i) at NSSTC in Huntsville, Alabama; (ii) at Emäsalo, Finland, during LPVEx; (iii) in central Oklahoma during MC3E; and (iv) at Rome, Italy, on the roof of one of the buildings of the "Sapienza" University of Rome during the HyMeX special observing period 1 (SOP 1). The MC3E dataset consists of data collected by five different two-dimensional video disdrometers deployed at a maximum distance of 9.2 km to be representative of the $5\,\mathrm{km} \times 5\,\mathrm{km}$ area that roughly corresponds to the footprint of the GPM dual-frequency precipitation radar (Hou et al. 2008). Table 1 summarizes the principal characteristics of each dataset including the period of

TABLE 1. Summary of 2DVD datasets.

Dataset	No. of devices	Period	Sample size (1-min DSD)	R_{mean} (mm h^{-1})	R_{max} (mm h^{-1})
NSSTC, Alabama	One 2DVD	Jul–Dec 2010	3257	2.26	187.49
LPVEx, Finland	One 2DVD	Sep–Oct 2010	3931	0.87	71.86
MC3E, Oklahoma	Five 2DVDs	Apr–May 2011	10 161	1.87	92.76
HyMeX, Italy	One 2DVD	Sep–Nov 2012	4760	2.53	152.46

the year when the measurements were collected, the number of devices deployed, the sample size of the dataset (i.e., the number of 1-min DSDs) after the use of the three different thresholds described above, and the mean and maximum value of the instantaneous measured rain rate.

The 2DVD data consist of different information on individual hydrometeors; specifically, for each drop that falls in the virtual measured area, the device measures the equivalent diameter (D in mm), the volume (V in mm^3), the fall speed (v; m s^{-1}), the oblateness, and the cross-sectional area (A; mm^2). Drop size distributions are computed from these data using

$$N(D_i) = \frac{1}{\Delta t \Delta D_i} \sum_{k=1}^{M_i} \frac{1}{A_k v_i}, \tag{10}$$

where Δt (s) is the time interval, ΔD_i (mm) is the width of the ith class of the DSD, and M_i is the total number of drops in the i bin. In the present work the DSDs are stratified in 50 bins with a constant width equal to 0.2 mm. The time interval is varied between 1 and 10 min. Using Eq. (10), 1-min DSDs were computed first. As mentioned above, the influence of the integration time on the assumption of the gamma distribution for fitting measured DSDs is investigated. For statistical comparison and to avoid the influence of the sample size on the final results, the moving average of the 1-min DSDs is implemented. In the study of Thurai et al. (2011) the time interval of the moving average was fixed to 3 min, while in this study it ranges from 2 to 10 min. Averaging in time, the fluctuation of the "instant" DSDs is reduced. In this way it is possible to obtain 10 samples of the same size (namely samples with the same number of DSDs): the first one is composed of 1-min DSDs, the second has the DSDs computed with the 2-min moving average, and the last one is composed of the DSDs averaged over 10-min time window.

Using the T-matrix method, the radar reflectivity ($Z_{h,m}$), the differential reflectivity ($Z_{dr,m}$), and the specific differential propagation phase ($K_{dp,m}$) were computed for each disdrometer-measured DSD along with the corresponding rain rate (R_m). Triplets of radar measurements were obtained at the frequencies of 2.725 (S band), 5.6 (C band), and 9.375 GHz (X band), at an environment temperature set to 20°C, using the assumption of PB, BC, Br, SL05, and SL07 shape–size models and Gaussian canting angle distribution with a mean of 0° and standard deviation of 10°. It is important to note that both radar observables and rain rate were computed directly from the disdrometer observations without assuming a particular DSD model.

b. *The simulated dataset of gamma DSDs*

The methodology described in section 3 requires a large dataset of gamma DSDs to enhance the probability of finding a gamma DSD of this dataset that is equivalent to a given measured one in the sense that determines the same radar measurements. The dataset was built by randomly varying the three parameters of Eq. (3a), namely N_w, D_0, and μ within some specified intervals. A frequently used interval for the mass-weighted drop median diameter is $0.5 \le D_0 \le 3.5$ mm, while the shape parameter μ ranges between -1 and 5, and the intercept parameter is simulated within $10^3 \le N_w \le 10^5$ mm^{-1} m^{-3}. Bringi and Chandrasekar (2001, section 8.1.1) and Gorgucci et al. (2008) used the above limits with the additional constraints of rain rates < 300 mm h^{-1} and $10 \log_{10} Z_h < 55$ dBZ at S band. However, other studies based on disdrometer data, such as Tokay and Short (1996), have highlighted a wider variability of gamma parameters, particularly N_w and μ. For the purpose of this study what counts is not to determine a "realistic" gamma DSD interval but an appropriately wide range of gamma DSD parameters to account for the variability of the radar measurement triplets determined from the disdrometer measured DSD, as described in section 4a.

Once the gamma-simulated DSDs were established, the radar measurements and the rain rate ($Z_{h,s}$, $Z_{dr,s}$, $K_{dp,s}$, and R_s) were computed using the same method and assumptions used to build the radar measurements from measured DSDs (section 4a). Further assumptions concern the limits of the gamma DSD that are set to $D_{min} = 0$ mm and $D_{max} = 10$ mm that correspond to the limit of the measured DSD.

A sensitivity study was performed to define a proper ranges of variability of the gamma parameters able to account for the variability of the measured dataset while keeping the size of the simulated dataset within an acceptable size for computing purposes. The ranges of

variability of the three gamma DSD parameters were investigated by gradually increasing the width of the range of each gamma parameter. Parameters are randomly chosen within their range of variability. For each set, the density of the points within the 3D space represented by the three radar dual-polarization measurements (Z_h, Z_{dr}, and K_{dp}) and the percentage of radar triplets obtained from measured DSDs that are included (i.e., CF < 0.001) within the simulated database were analyzed. For example, for the ranges of gamma DSD parameters mentioned above, and the BC shape model, the percentage of gamma triplets with the nearest triplet within a CF ≤ 0.001 is around 99%. This fact allows us to consider the density of the triplets as appropriate. Other drop shape–size models present similar results.

However, a major problem is that for a relatively large number of radar triplets obtained from the measured DSD datasets the methodology proposed in section 3 is not able to find a match in the simulated gamma dataset because the value of the cost function Eq. (9) is higher than the imposed limit. This is due not to the matching criteria, but to the fact that radar measurements were outside the chosen ranges of variability. Considering the NSSTC dataset, the triplets obtained from measured DSDs that do not find the corresponding matching triplet in the gamma DSD dataset are around 20% of the dataset, depending on the integration time considered. Therefore, the interval of gamma DSDs must be widened.

As expected, by increasing the range of gamma DSD parameters, the percentage of measured DSDs that can find a corresponding gamma DSD in the simulated dataset increases. The parameter that has the most influence on these results is N_w. Of course, when increasing the width of the range, keeping fixed the population of dataset, the density of the triplets of the database decreases. Increasing the number of triplets causes the density to increase but the computing time also consequently increases. After the analysis of the results of the sensitivity study, the following ranges were used to obtain the simulated gamma DSD dataset used in this paper:

$$\begin{aligned} &10^1 \leq N_w \leq 10^7 \quad (\mathrm{mm}^{-1}\,\mathrm{m}^{-3}),\\ &0.5 \leq D_0 \leq 3.5 \quad (\mathrm{mm}), \quad \text{and}\\ &-4 \leq \mu \leq 20. \end{aligned} \tag{11}$$

More than 80 000 gamma DSDs were generated by randomly choosing triplets in Eq. (11). Considering 0.001 (see section 3) as the minimum acceptable distance between the triplets, the percentage of the gamma triplets that have at least one neighboring triplet within this distance is 99.76%. This means that the density of the dataset is acceptable for the purpose of this study. The percentage of the radar measurement triplets computed from the measured DSDs that are not included in the dataset of the simulated triplets is another parameter considered for selecting the width of the range of variability of the gamma parameters. Depending on the shape–size model and the integration time considered, the latter percentage varies, but obtained values are usually lower than 3%. However, the values of CF of the measured DSDs that are not included in the gamma DSD dataset are often just slightly greater than the selected threshold. Moreover, the discharged measured DSDs have in common a high value of the horizontal reflectivity, close to the limit of 55 dBZ. Hereafter the dataset generated as described above is referred to as the *gamma-simulated dataset*.

5. Results

a. Simulated dataset

The method described in section 3 aims to identify pairs of DSDs, one measured and one gamma that are equivalent from the viewpoint of radar measurements. These radar-equivalent DSD pairs will not necessarily be equivalent for other properties such as the rain rate, whose quantitative measurement is instead the objective of retrieval techniques based on radar measurements. Focusing on rain rate, we would ascribe the difference between the rain rates of the two DSDs of each pair to the limited validity of assumption that the natural DSD follows a three-parameter gamma distribution. To ascertain this point, we need (i) to verify that the methodology described in section 3 determines negligible differences in rain rates if applied to a dataset of gamma DSD, and (ii) to estimate the effect of disdrometer sampling errors. We try to assess point i using theoretical gamma DSD and point ii using a simulation of disdrometer observations of gamma DSD.

To address the first issue, the jackknife method (Quenouille 1956; Tukey 1958) was used. For each gamma DSD of the gamma-simulated dataset, the proposed methodology was applied using the dataset composed of all the gamma-simulated DSDs except the given one. Then the cost function was computed and if its value was less than 0.001, the interpolating function was evaluated. Finally, the quality control was applied. Once the gamma-simulated DSD with the three radar measurements closest to the radar triplet of the given DSD was identified, the values of the rain rate of the two DSDs were computed and compared. The normalized standard error (NSE), defined as the standard deviation normalized with respect to the mean, and the normalized bias (NB) are the statistical estimators used to evaluate the differences between rain rates. The results for the BC

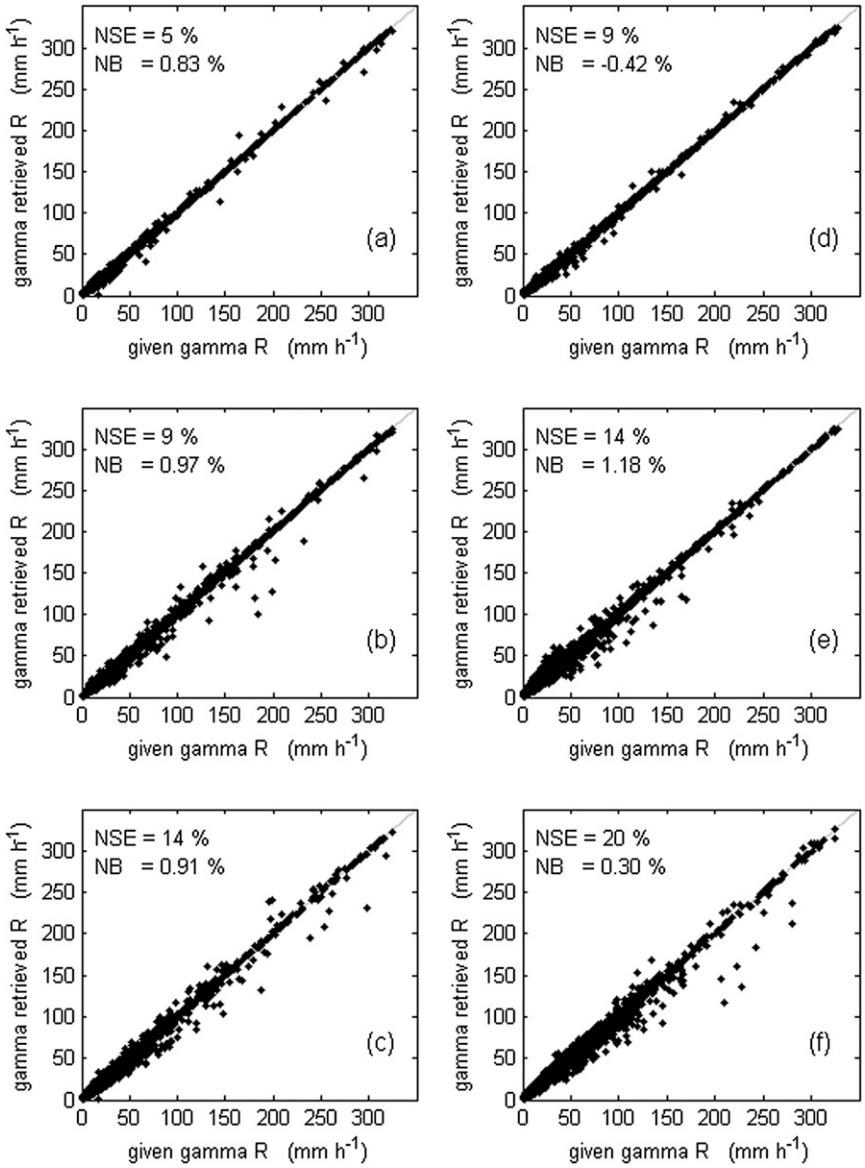

FIG. 3. Comparison between the rain rate of a given gamma-simulated DSD and that of (left) the gamma-simulated DSD and (right) the disdrometer-simulated DSD determined with the method in Fig. 1. The results are obtained considering the BC shape–size model and the (a),(d) S band, (b),(e) C band, and (c),(f) X band.

shape model are shown in Fig. 3 for S band (Fig. 3a), C band (Fig. 3b), and X band (Fig. 3c). The NSEs are 5% for S band, 9% for C band, and 14% for X band. The normalized biases are 0.83%, 0.97%, and 0.91% for S, C, and X band, respectively, and therefore the method can be considered unbiased.

To identify the influence of the disdrometer sampling error, the methodology presented in section 3 has been applied to gamma DSD as resulting from disdrometer sampling. The procedure followed for the generation of the disdrometer-simulated dataset of gamma DSD is the same described in Chandrasekar and Bringi (1987) and used in other studies (e.g., Smith et al. 1993; Smith and Kliche 2005; Moisseev and Chandrasekar 2007). Starting from the gamma-simulated dataset, a simulation of disdrometer rainfall observations has been performed to obtain a *disdrometer-simulated dataset* based on two assumptions: (i) the number of drops in a given volume follows the Poisson distribution and (ii) the diameters of those drops follow the gamma distribution. For this simulation we have assumed a sampling area of 100 cm^2 like that of 2DVD, a sampling interval of 60 s, and

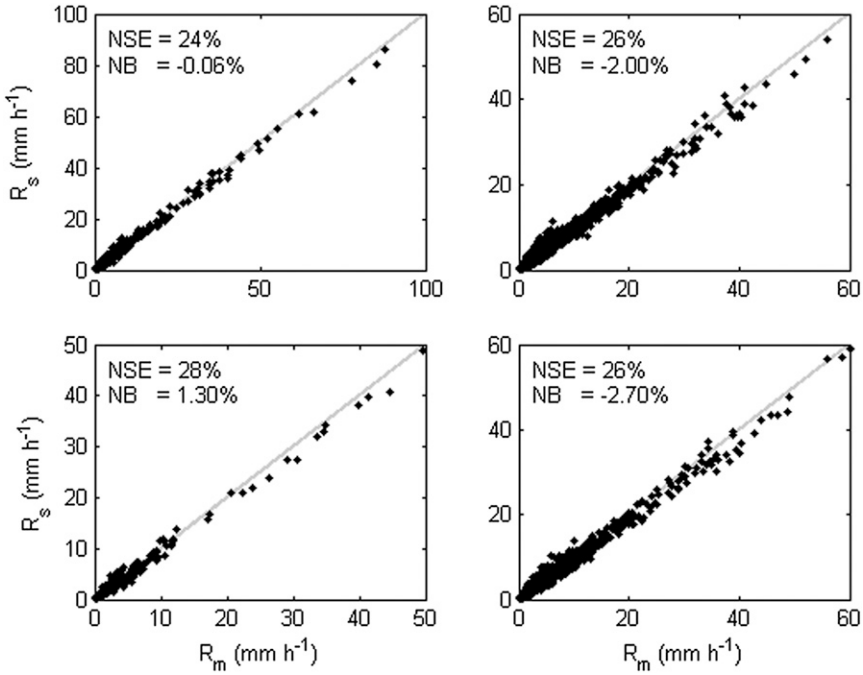

FIG. 4. Rain rate computed for 1-min 2DVD-measured DSD vs rain rate computed from gamma DSD estimated with the procedure described in Fig. 1. Results were obtained considering S band and the shape model of BC for each dataset: (top left) NSSTC dataset, (top right) MC3E dataset, (bottom left) LPVEx dataset, and (bottom right) HyMeX dataset.

a mean raindrop velocity of $5\,\mathrm{m\,s^{-1}}$. Moisseev and Chandrasekar (2007) pointed out that using a constant sampling volume for all diameters does not affect the results; therefore in this study we assume that the fall velocity does not vary with the raindrop size. Then, for each of these DSDs, the gamma-simulated DSD that gives the same triplet of radar measurements has been found. The resulting values of NSE and NB of rain rates relative to the two DSDs take into account both the error due to the proposed DSD matching methodology and disdrometer sampling error. Figure 3 shows the results obtained for the BC shape model and for S band (Fig. 3d), C band (Fig. 3e), and X band (Fig. 3f). The values of NSE are 9% for S band, 14% for C band, and 20% for X band, while the normalized bias are −0.42%, 1.18%, and 0.30%, respectively. The still negligible NB implies that sampling errors of disdrometers do not have a strong influence of the performance of the method applied to gamma DSD. Values of NSE show a small increase with respect to the case of continuous gamma DSD.

b. Experimental datasets

The methodology described in section 3 was finally applied to the four datasets (see section 4a) of two-dimensional video disdrometer measurements. For each measured DSD, the corresponding gamma DSD is obtained based on the fact that it determines the same dual-polarization radar measurements. Two series containing the rain rates computed directly from both the measured and gamma DSD can be obtained and compared through NB and NSE. To evaluate properties such as the median and the confidence interval of NB and NSE, the bootstrapping method (Efron 1979) is adopted. The aim is to determine those properties sampling from an approximating distribution that, in the present work, is the empirical distribution of the NSE and NB of the two series of rain rate obtained by applying the method described in section 3. The aim has been achieved by constructing a thousand resamples of the original dataset, each with the same size and obtained by random sampling with replacements from the original dataset.

As example of a measured dataset, a scatterplot of the rain rate measured versus the gamma-simulated rain rate is presented in Fig. 4 considering 1-min DSDs, S band, and the shape model of BC. An identity line is drawn as a reference. As expected, there is a certain agreement between the two distributions, that is, the pattern of dots clustered along the identity line, indicating that rainfall rates from the equivalent gamma DSDs are almost unbiased, even though certain dispersion is also evident. In the scatterplots showed in Fig. 4, the values of NSE for the NSSTC, MC3E, LPVEx, and HyMeX datasets are

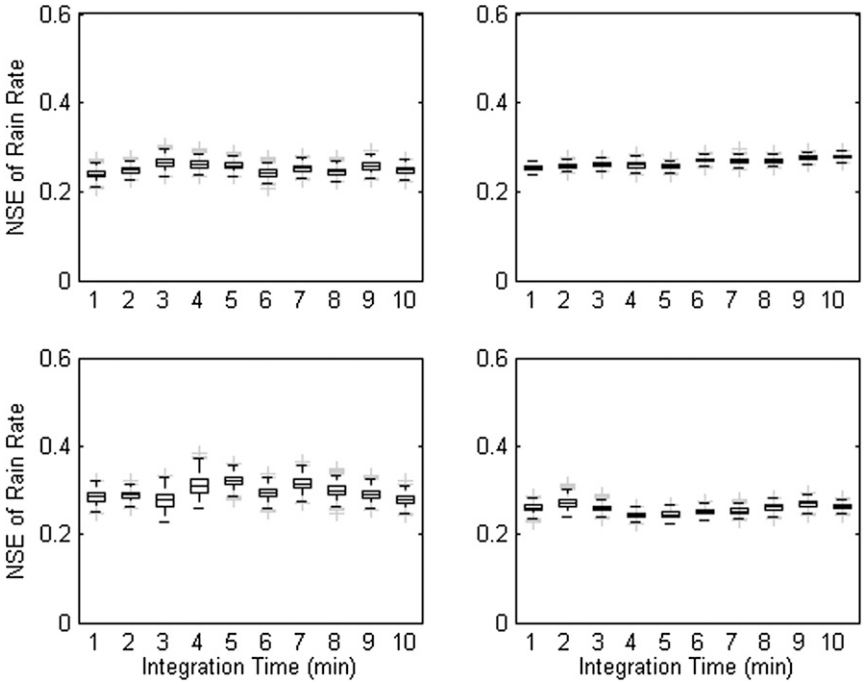

FIG. 5. Box plots of the values of NSE between measured and simulated rain rate at S band for the BC shape model and varying the integration time: (top left) NSSTC dataset, (top right) MC3E dataset, (bottom left) LPVEx dataset, and (bottom right) HyMeX dataset.

24%, 26%, 28%, and 26%, respectively, while the values of the NB are −0.06%, −2.0%, 1.3%, and −2.7%, respectively. Although there are some differences, results are similar for all the datasets. As verified using different integration intervals and shape models the bias is negligible, but it is not possible to assert the same for the value of NSE, which is greater than the error (9%) associated with retrieving a disdrometer-measured gamma DSD, as shown in the previous section. Therefore, part of this error is related to the fact that the given measured DSD is not gamma. Cao and Zhang (2009) used the bias and the fractional error to evaluate the error in rain rate with disdrometer measurements obtaining lower values of error with respect to the proposed method. For example, using method of moments with different moment sets, their fractional error ranges between 0.05% of fourth, fifth, and sixth moments and 7.38% of zeroth, first, and second moments (we found similar fractional errors by applying these method to our measured datasets). Such errors are lower with respect those obtained in our study (in terms of fractional error they are 14%, 14%, 12%, and 15% for NSSTC, MC3E, LPVEx, and HyMeX, respectively). Such difference can be partially ascribed to the matching method but principally ascribed to the choice of using radar measurements.

A more detailed analysis is performed for the four datasets by varying the integration interval and the shape–size model. The procedure used to integrate the DSDs over longer time intervals is shown in section 4a, while the shape–size relations used are reported in section 2. Figure 5 shows the box plots of values of NSE between measured rain and rain from gamma DSDs considering different sampling time and datasets for the BC shape model and the S-band frequency obtained using the bootstrap method described above. For each box, the central mark is the median, the edges of the box are the 25th and 75th percentiles, the whiskers represent the ±2.7 standard deviations, and the crosses are the outliers. Considering all the datasets, the values of NSE range between 22% and 32% except for a few cases. In terms of trend and values there is not a big difference between the different datasets, even though the four datasets were collected in four different climatic areas of the word. The trends of the median values of NSE are roughly smooth, indicating there is not an important influence from the integration time on the computation of the rain rate using a gamma DSD model. Therefore, considering longer time intervals, the representativeness of the gamma model does not change significantly. Very little spacing between the median and the 25th and 75th percentiles median is detected; thus, the dispersion of the values of NSE is low.

The other estimator used in this study is the normalized bias; Fig. 6 shows the results obtained for S band

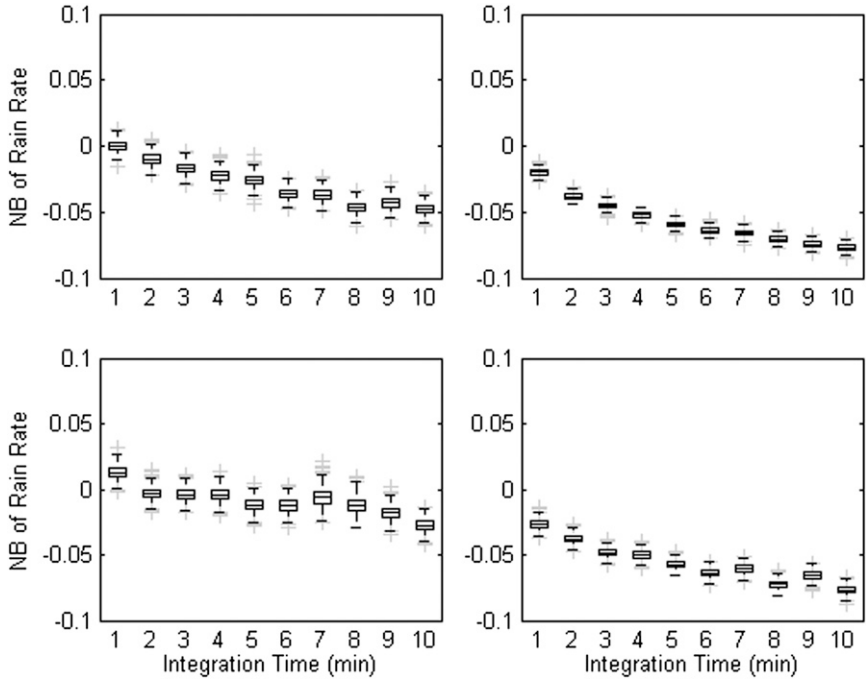

FIG. 6. As in Fig. 5, but for values of NB.

with increasing time intervals and for the shape–size model of BC. The order of magnitude of the NB is lower than the normalized standard errors and is never greater than 10%. In most of the cases the NBs have negative values. Therefore, fitting the drop size distributions with a three-parameter gamma distribution underestimates the rain rate. The NBs have a well-defined trend, their absolute values slightly increasing with increasing integration time. Also, for the normalized bias the dispersion of the values around the median is weak.

To study the influence of the shape model, the methodology was applied to datasets built using the different shape models mentioned in section 2. Considering the S band, the trends of the median of the two estimators are shown in Figs. 7 and 8 and are in accordance with what was found using the shape model of BC. However, some differences among the results obtained with the different shape–size models were found. Because, in all the datasets considered, the lowest values of NSE were obtained using the linear shape models, it is possible to deduce that using those, the influence of assuming a gamma DSD for describing natural drop size distribution has a more limited impact on radar measurements. The highest NSE was found with the Br model.

Finally, the impact on the method of using weather radars at different wavelengths has been investigated. The analysis performed for S band was repeated for the experimental and gamma datasets using the T-matrix method with the same assumptions to generate polarimetric radar measurements at C and X band. For the BC model, the values of NSE and NB obtained for C band are plotted in Figs. 9 and 10, respectively. The mean values of NSE for C band are a few percentage points higher than the S band, but the trends are similar, thus confirming the independence of the results from the integration time interval. A slightly greater dispersion of the values on NSE around the medians is evident and this effect can be attributed to the fact that at C band the resonance scattering is more significant compared to S band. Analyzing the values of normalized bias, the effects resulting from the use of a different frequency band are of minor importance. In fact, for C band, as well as for S band, the values of normalized bias are lower than 10%, in most of the cases negative, and the absolute values increase as the integration time is increased. Similar results were obtained using X band for the computation of the radar measurements and are shown in Figs. 11 and 12 for the normalized standard error and for the normalized bias.

6. Summary and conclusions

This study aimed to analyze the error of assuming that a natural DSD follows the three-parameter gamma distribution. The error is evaluated by computing rainfall rates obtained from two DSDs, one measured and one

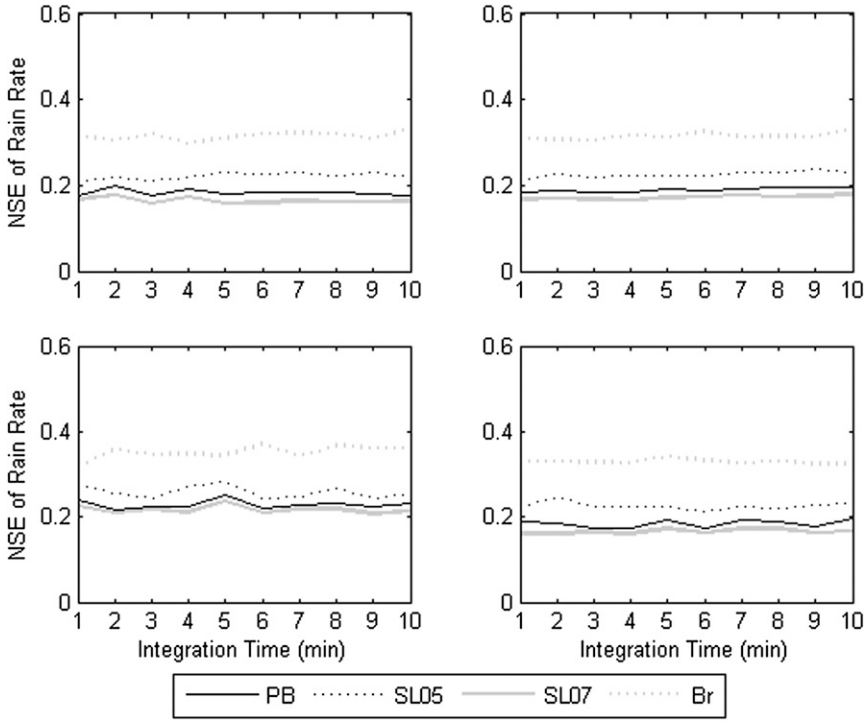

FIG. 7. Values of NSE between measured and simulated rain rate for four different shape models (PB, SL05, SL07, and Br) in the S band and varying the integration time: (top left) NSSTC dataset, (top right) MC3E dataset, (bottom left) LPVEx dataset, and (bottom right) HyMeX dataset.

gamma, that are equivalent from the point of view of the radar measurements Z_h, Z_{dr}, and K_{dp}. Assuming that a given triplet of intrinsic Z_h, Z_{dr}, and K_{dp}—once some constraints such as drop shape–size relation, temperature, and canting are fixed—is representative of only one gamma DSD, a methodology was developed to identify such a gamma DSD that, at a specific frequency, determines the same dual-polarization radar measurements. Rain rates of the two DSDs, however, can be different, and that difference can be used as a means to quantify the error related to assuming a gamma form for DSDs. Since each simulated DSD is defined by three raindrop size distribution parameters (see section 4b), the procedure used to match measured DSDs and gamma DSDs could be seen as a further new method for fitting gamma parameters using dual-polarization radar data. Actually, to compare this with other fitting methods is out of the scope of this study, which is the validity of assuming gamma DSDs, and would require taking into account other issues, such as the influence of radar measurement error. The intrinsic error of the proposed method is evaluated in terms of rain rate once it is applied to widely varying gamma-simulated DSDs using a jackknife approach. Results show that the error depends on the frequency and, in terms of NSE, is 5%, 9%, and 14% for S, C, and X band, respectively. The influence of the disdrometer sampling error is analyzed applying the proposed matching methodology to a gamma DSD dataset resulting after simulating disdrometer sampling. The obtained NSE and NB depend both on the error due to the method and on the sampling error. The NSE is 9% for S band, 14% for C band, and 20% for X band.

Finally, the proposed method was applied to the data collected by two-dimensional video disdrometers located in four different climate regions around the world. Datasets of experimental DSDs are produced with time intervals varying from 1 to 10 min. After the application of a filter criterion for the detection and removal of the outliers, and of thresholds to define rain/no rain conditions, the proposed methodology was applied to match gamma DSDs that are equivalent from the point of view of radar measurements to an experimental DSD. The corresponding values of rain rates retrieved from the gamma and the measured DSD are analyzed in terms of statistical estimators NB and NSE whose confidence is evaluated by a bootstrapping method.

The results were discussed considering different shape models, different radar frequencies, and different integration time intervals. The trends of the values of the normalized standard error and normalized bias for the

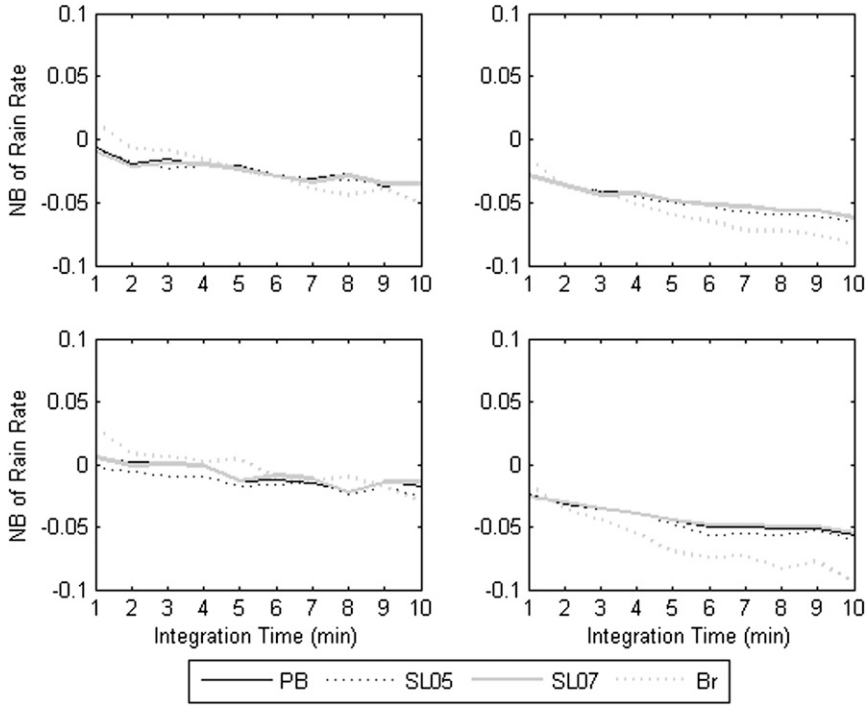

FIG. 8. As in Fig. 7, but for values of NB.

different shape models (shown only for S band) considered in this study are comparable, although for the linear shape models lower values of NSE are registered. Considering the normalized standard error, the effects of the frequency band are more evident. For C band there is a greater dispersion of the values around the medians, and the NSE is, on average, greater than for S band. The median values of NSE range around 26%

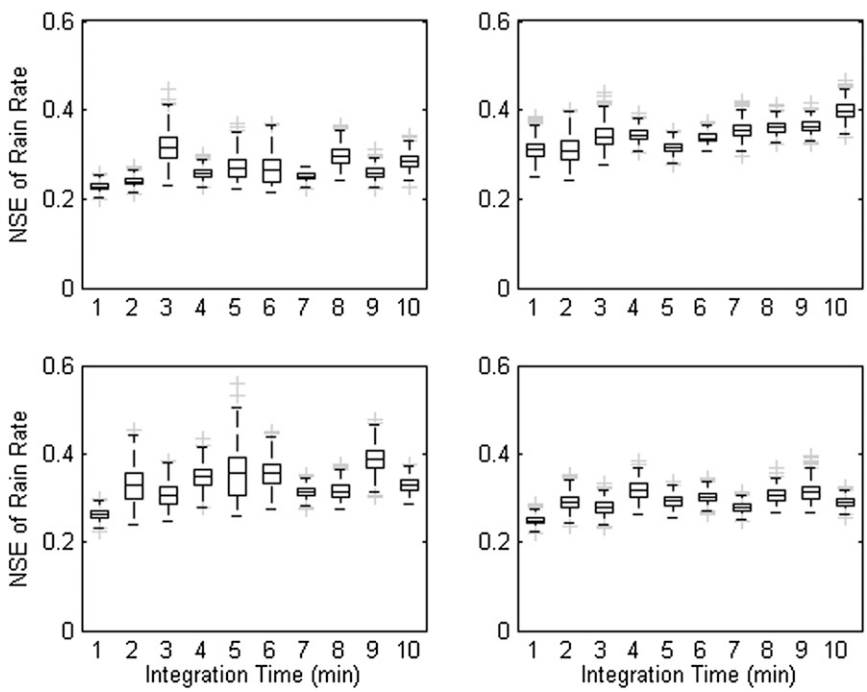

FIG. 9. As in Fig. 5, but for the C band.

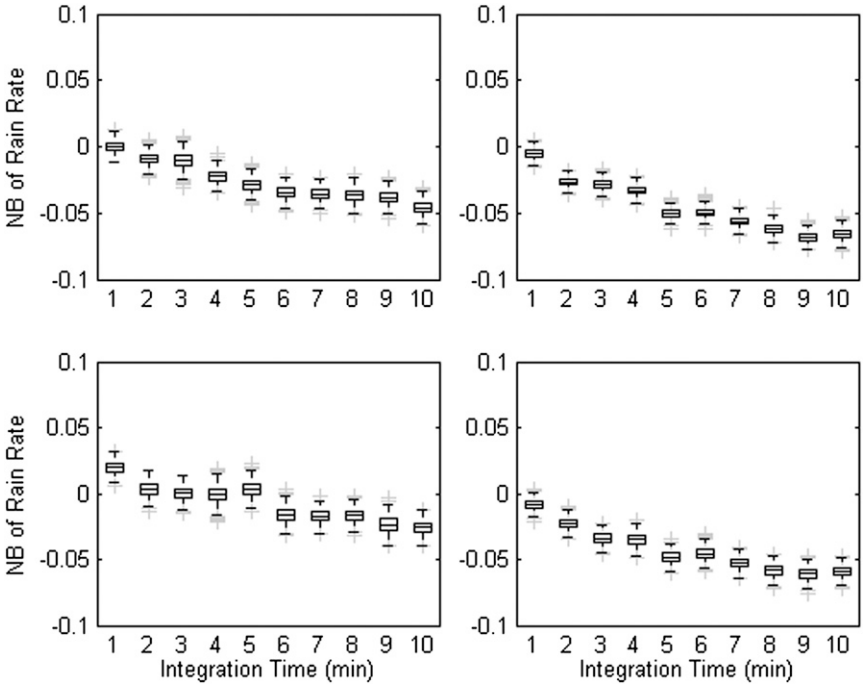

FIG. 10. As in Fig. 6, but for the C band.

and 30%, respectively, for S band and C band, while for X band, considering the four datasets, the mean value of NSE is 33%. If the same radar measurements are obtained from a natural and a gamma DSD, the difference between rain rates associated with the two DSDs presents a nonnegligible NSE that can be related to differences of the shape of the two DSDs and not to the DSD matching procedure that yields lower NSE (values

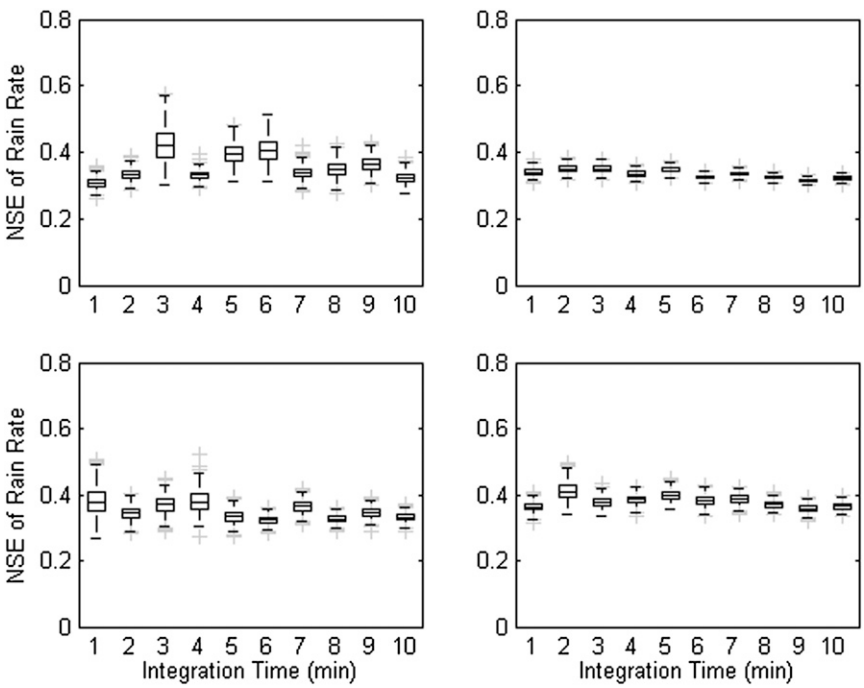

FIG. 11. As in Fig. 5, but for X band.

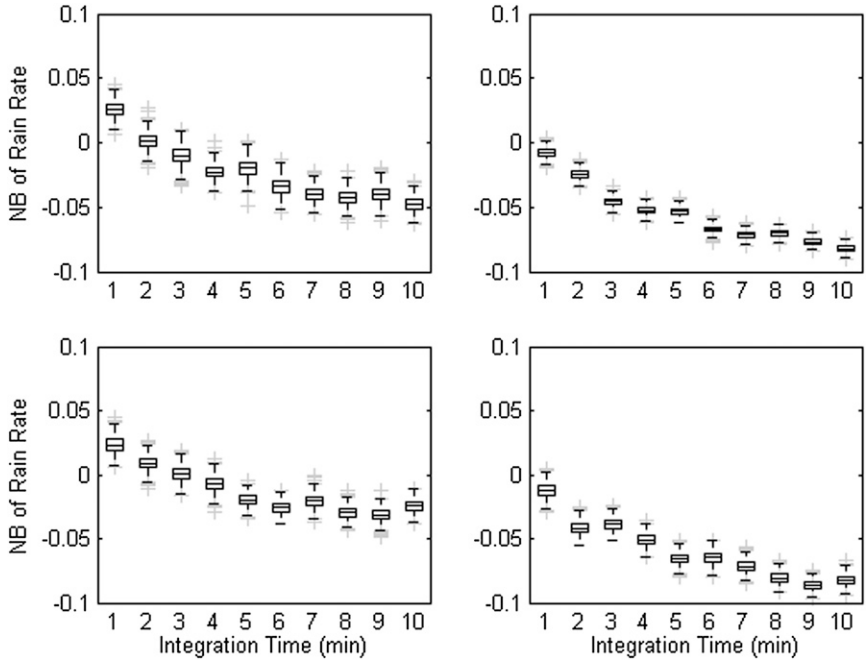

FIG. 12. As in Fig. 6, but for X band.

in Figs. 3d–f). Last, the NSE of the two distributions of rain rates depends on the drop shape–size model adopted, while the absolute value of normalized bias increases as the integration time increases.

In this study, the four datasets of disdrometer measurements were investigated as a whole. Further investigations would aim to identify conditions determining deviations of measured DSD from the gamma functional form. The proposed methodology can be used to test the validity of other DSD functional forms, including truncated or constrained gamma.

Acknowledgments. This research was partially supported by the Italian Department of Civil Protection and NASA Precipitation Measurement Mission (PMM) NNX10AJ12G under Ramesh Kakar, program scientist, NASA Headquarters. The authors acknowledge the anonymous reviewers for their detailed and helpful comments to the manuscript. The 2DVD measurements used in this study were collected during a 6-month-long field campaign in Huntsville, Alabama; LPVEx in Finland; MC3E in Oklahoma; and finally during the HyMeX SOP 1 in Rome, Italy, when the NASA 2DVD was set up at the Laboratory of Radio Meteorology of Sapienza University of Rome (Prof. F. S. Marzano). The authors acknowledge the NASA GPM mission ground validation program under Matthew Schwaller, GPM ground validation manager, and Walter A. Petersen, GPM ground validation science manager, for providing 2DVD data and contributions to the HyMeX field campaign. Acknowledgments extend to Arthur Hou (deceased), former GPM project scientist, for his vision throughout the GPM core-satellite prelaunch activities.

REFERENCES

Adirosi, E., L. Baldini, F. Lombardo, F. Russo, and F. Napolitano, 2013: Comparison of different fittings of experimental DSD. *AIP Conf. Proc.,* **1558,** 1669, doi:10.1063/1.4825850.

Barber, P.-W., and C. Yen, 1975: Scattering of electromagnetic waves by arbitrarily shaped dielectric bodies. *Appl. Opt.,* **14,** 2864–2872, doi:10.1364/AO.14.002864.

Beard, K. V., and C. Chuang, 1987: A new model for the equilibrium shape of raindrops. *J. Atmos. Sci.,* **44,** 1509–1524, doi:10.1175/1520-0469(1987)044<1509:ANMFTE>2.0.CO;2.

——, V. N. Bringi, and M. Thurai, 2010: A new understanding of raindrop shape. *Atmos. Res.,* **97,** 396–415, doi:10.1016/j.atmosres.2010.02.001.

Best, A. C., 1950: The size distribution of raindrops. *Quart. J. Roy. Meteor. Soc.,* **76,** 16–36, doi:10.1002/qj.49707632704.

Brandes, E. A., G. Zhang, and L. Vivekanandan, 2002: Experiments in rainfall estimation with a polarimetric radar in a subtropical environment. *J. Appl. Meteor.,* **41,** 674–685, doi:10.1175/1520-0450(2002)041<0674:EIREWA>2.0.CO;2.

Bringi, V. N., and V. Chandrasekar, 2001: *Polarimetric Doppler Weather Radar Principles and Applications.* Cambridge University Press, 648 pp.

——, ——, J. Hubbert, E. Gorgucci, W. L. Randeu, and M. Schoenhuber, 2003: Raindrop size distribution in different climatic regimes from disdrometer and dual-polarized radar analysis. *J. Atmos. Sci.,* **60,** 354–365, doi:10.1175/1520-0469(2003)060<0354:RSDIDC>2.0.CO;2.

Cao, Q., and G. Zhang, 2009: Errors in estimating raindrop size distribution parameters employing disdrometer and simulated raindrop spectra. *J. Appl. Meteor. Climatol.,* **48,** 406–425, doi:10.1175/2008JAMC2026.1.

——, ——, E. A. Brandes, T. Schuur, A. Ryzhkov, and K. Ikeda, 2008: Analysis of video disdrometer and polarimetric radar data to characterize rain microphysics in Oklahoma. *J. Appl. Meteor. Climatol.,* **47,** 2238–2255, doi:10.1175/2008JAMC1732.1.

Caracciolo, C., F. Prodi, A. Battaglia, and F. Porcu', 2006: Analysis of the moments and parameters of a gamma DSD to infer precipitation properties: A convective stratiform discrimination algorithm. *Atmos. Res.,* **80,** 165–186, doi:10.1016/j.atmosres.2005.07.003.

Chandrasekar, V., and V. N. Bringi, 1987: Simulation of radar reflectivity and surface measurements of rainfall. *J. Atmos. Oceanic Technol.,* **4,** 464–478, doi:10.1175/1520-0426(1987)004<0464:SORRAS>2.0.CO;2.

Delaunay, D., 1934: Sur la sphère vide. *Izv. Akad. Nauk SSSR,* **7,** 793–800.

Efron, B., 1979: Bootstrap methods: Another look at jackknife. *Ann. Stat.,* **7,** 1–26, doi:10.1214/aos/1176344552.

Feingold, G., and Z. Levin, 1986: The lognormal fit to raindrop spectra from frontal convective clouds in Israel. *J. Climate Appl. Meteor.,* **25,** 1346–1363, doi:10.1175/1520-0450(1986)025<1346:TLFTRS>2.0.CO;2.

Gorgucci, E., G. Scarchilli, V. Chandrasekar, and V. N. Bringi, 2000: Measurement of mean raindrop shape from polarimetric radar observations. *J. Atmos. Sci.,* **57,** 3406–3413, doi:10.1175/1520-0469(2000)057<3406:MOMRSF>2.0.CO;2.

——, V. Chandrasekar, and L. Baldini, 2008: Microphysical retrievals from dual-polarization radar measurements at X band. *J. Atmos. Oceanic Technol.,* **25,** 729–741, doi:10.1175/2007JTECHA971.1.

Gunn, K. L. S., and J. S. Marshall, 1955: The effect of wind shear on falling precipitation. *J. Meteor.,* **12,** 339–349, doi:10.1175/1520-0469(1955)012<0339:TEOWSO>2.0.CO;2.

Gunn, R., and G. D. Kinzer, 1949: The terminal velocity of fall for water droplets in stagnant air. *J. Meteor.,* **6,** 243–248, doi:10.1175/1520-0469(1949)006<0243:TTVOFF>2.0.CO;2.

Hosking, J. R. M., 1990: L-moments: Analysis and estimation of distributions using linear combinations of order statistics. *J. Roy. Stat. Soc.,* **52B,** 105–124.

Hou, A. Y., G. Skofronick-Jackson, C. D. Kummerow, and J. M. Shepher, 2008: Global precipitation measurements. *Precipitation Advances in Measurement, Estimation and Prediction,* S. Michaelides, Ed., Springer, 131–164.

Ignaccolo, M., and C. De Michele, 2014: Phase space parameterization of rain: The inadequacy of gamma distribution. *J. Appl. Meteor. Climatol.,* **53,** 548–562, doi:10.1175/JAMC-D-13-050.1.

Joss, J., and E. G. Gori, 1978: Shapes of raindrop size distribution. *J. Appl. Meteor.,* **17,** 1054–1061, doi:10.1175/1520-0450(1978)017<1054:SORSD>2.0.CO;2.

Kliche, D. V., P. L. Smith, and R. W. Johnson, 2008: L-moment estimators as applied to gamma drop size distributions. *J. Appl. Meteor. Climatol.,* **47,** 3117–3130, doi:10.1175/2008JAMC1936.1.

Kozu, T., and K. Nakamura, 1991: Rain parameter estimation from dual-radar measurements combining reflectivity profile and path-integrated attenuation. *J. Atmos. Oceanic Technol.,* **8,** 259–270, doi:10.1175/1520-0426(1991)008<0259:RPEFDR>2.0.CO;2.

Marshall, J. S., and W. M. Palmer, 1948: The distribution of raindrops with size. *J. Meteor.,* **9,** 327–332.

Moisseev, D., and V. Chandrasekar, 2007: Nonparametric estimation of raindrop size distributions from dual-polarization radar spectral observations. *J. Atmos. Oceanic Technol.,* **24,** 1008–1018, doi:10.1175/JTECH2024.1.

Nešpor, V., W. F. Krajewski, and A. Kruger, 2000: Wind-induced error of raindrop size distribution measurement using a two-dimensional video disdrometer. *J. Atmos. Oceanic Technol.,* **17,** 1483–1492, doi:10.1175/1520-0426(2000)017<1483:WIEORS>2.0.CO;2.

Pruppacher, H. R., and K. V. Beard, 1970: A wind investigation of the internal circulation and shape of water drops falling at terminal velocity in air. *Quart. J. Roy. Meteor. Soc.,* **96,** 247–256, doi:10.1002/qj.49709640807.

Quenouille, M. H., 1956: Notes on bias in estimation. *Biometrika,* **43,** 353–36.

Schönhuber, M., G. Lammer, and W. L. Randeu, 2007: One decade of imaging precipitation measurement by 2D-video-disdrometer. *Adv. Geosci.,* **10,** 85–90, doi:10.5194/adgeo-10-85-2007.

——, ——, and ——, 2008: The 2D video disdrometer. *Precipitation Advances in Measurement, Estimation and Prediction,* S. Michaelides, Ed., Springer, 3–31.

Sempere Torres, D., J. M. Porrà, and J. D. Creutin, 1994: A general formulation for raindrop size distribution. *J. Appl. Meteor.,* **33,** 1494–1502, doi:10.1175/1520-0450(1994)033<1494:AGFFRS>2.0.CO;2.

Smith, P. L., and D. Kliche, 2005: The bias in moment estimators for parameters of drop size distribution functions: Sampling from exponential distributions. *J. Appl. Meteor.,* **44,** 1195–1205, doi:10.1175/JAM2258.1.

——, Z. Liu, and J. Joss, 1993: A study of sampling-variability effects in raindrop size observations. *J. Appl. Meteor.,* **32,** 1259–1269, doi:10.1175/1520-0450(1993)032<1259:ASOSVE>2.0.CO;2.

——, D. Kliche, and R. W. Johnson, 2009: The bias and error in moment estimators for parameters of drop size distribution functions: Sampling from gamma distributions. *J. Appl. Meteor. Climatol.,* **48,** 2118–2126, doi:10.1175/2009JAMC2114.1.

Thurai, M., W. A. Petersen, A. Tokay, C. Schultz, and P. Gatlin, 2011: Drop size distribution comparisons between Parsivel and 2-D video disdrometers. *Adv. Geosci.,* **30,** 3–9, doi:10.5194/adgeo-30-3-2011.

——, V. Bringi, W. Petersen, and P. Gatlin, 2013: Drop shapes and fall speeds in rain: Two contrasting examples. *J. Appl. Meteor. Climatol.,* **52,** 2567–2581, doi:10.1175/JAMC-D-12-085.1.

Tokay, A., and D. A. Short, 1996: Evidence from tropical raindrop spectra of the origin of rain from stratiform and convective clouds. *J. Appl. Meteor.,* **35,** 355–371, doi:10.1175/1520-0450(1996)035<0355:EFTRSO>2.0.CO;2.

——, A. Kruger, and W. Krajewski, 2001: Comparison of drop-size distribution measurements by impact and optical disdrometers. *J. Appl. Meteor.,* **40,** 2083–2097, doi:10.1175/1520-0450(2001)040<2083:CODSDM>2.0.CO;2.

——, W. A. Petersen, P. Gatlin, and M. Wingo, 2013: Comparison of raindrop size distribution measurements by collocated disdrometers. *J. Atmos. Oceanic Technol.,* **30,** 1672–1690, doi:10.1175/JTECH-D-12-00163.1.

Tukey, J. W., 1958: Bias and confidence in not-quite large samples. *Ann. Math. Stat.,* **29,** 614–623, doi:10.1214/aoms/1177706647.

Ulbrich, C., 1983: Natural variations in the analytical form of the raindrop-size distribution. *J. Climate Appl. Meteor.,*

22, 1764–1775, doi:10.1175/1520-0450(1983)022<1764:NVITAF>2.0.CO;2.

——, 1985: The effects of drop size distribution truncation on rainfall integral parameters and empirical relations. *J. Climate Appl. Meteor.,* **24,** 580–590, doi:10.1175/1520-0450(1985)024<0580:TEODSD>2.0.CO;2.

Willis, P. T., 1984: Functional fits to some observed drop size distributions and parameterization of rain. *J. Atmos. Sci.,* **41,** 1648–1661, doi:10.1175/1520-0469(1984)041<1648:FFTSOD>2.0.CO;2.

Zhang, G., J. Vivekanandan, E. A. Brandes, R. Meneghini, and T. Kozu, 2003: The shape–slope relation in observed gamma raindrop size distributions: Statistical error or useful information? *J. Atmos. Oceanic Technol.,* **20,** 1106–1119, doi:10.1175/1520-0426(2003)020<1106:TSRIOG>2.0.CO;2.

——, S. Luchs, A. Ryzhkov, M. Xue, L. Ryzhkova, and Q. Cao, 2011: Winter precipitation microphysics characterized by polarimetric radar and video disdrometer observations in central Oklahoma. *J. Appl. Meteor. Climatol.,* **50,** 1558–1570, doi:10.1175/2011JAMC2343.1.